615859

AIAA 2002-2516

A Method for Optimizing Non-Axisymmetric Liners For Multimodal Sound Sources

W. R. Watson, M. G. Jones,
T. L. Parrott, and J. Sobieski
NASA Langley Research Center
Hampton, VA 23681-2199

8th AIAA/CEAS Aeroacoustics Conference
June 17-19, 2002
Breckenridge, Colorado

A METHOD FOR OPTIMIZING NON-AXISYMMETRIC LINERS FOR MULTIMODAL SOUND SOURCES

W. R. Watson*, M. G. Jones†, T. L. Parrott‡ and J. Sobieski§
NASA Langley Research Center, Hampton, Virginia 23681-2199

Abstract

Central processor unit times and memory requirements for a commonly used solver are compared to that of a state-of-the-art, parallel, sparse solver. The sparse solver is then used in conjunction with three constrained optimization methodologies to assess the relative merits of non-axisymmetric versus axisymmetric liner concepts for improving liner acoustic suppression. This assessment is performed with a multimodal noise source (with equal mode amplitudes and phases) in a finite-length rectangular duct without flow. The sparse solver is found to reduce memory requirements by a factor of five and central processing time by a factor of eleven when compared with the commonly used solver. Results show that the optimum impedance of the uniform liner is dominated by the least attenuated mode, whose attenuation is maximized by the Cremer optimum impedance. An optimized, four-segmented liner with impedance segments in a checkerboard arrangement is found to be inferior to an optimized spanwise segmented liner. This optimized spanwise segmented liner is shown to attenuate substantially more sound than the optimized uniform liner and tends to be more effective at the higher frequencies. The most important result of this study is the discovery that when optimized, a spanwise segmented liner with two segments gives attenuations equal to or substantially greater than an optimized axially segmented liner with the same number of segments.

Nomenclature

$[A]$	= system matrix
A_{qm}	= rigid-wall duct mode coefficients, Pa
$\{B\}$	= vector of source effects, Pa
c_0	= sound speed in duct, m/s
E	= axial acoustic intensity, Pa m/s
F	= noise suppression, dB
f	= source frequency, Hz
H, W, L	= height, width, and length of duct, m
i	$= \sqrt{-1}$
k	$= (\omega/c_0)$, freespace wavenumber, m^{-1}
NX	= number of transverse grid points
NY	= number of spanwise grid points
NZ	= number of axial grid points
p	= time independent acoustic pressure, Pa
R, χ	= normalized acoustic resistance and reactance
t	= dimensional time, s
x, y, z	= transverse, spanwise, and axial coordinate, m
$\mathrm{Re}\{\ \}$	= real part of complex expression
ζ	$= R + i\chi$, normalized acoustic impedance
∇^2	= three-dimensional Laplace operator, m^{-2}
$\frac{\partial p}{\partial n}$	= normal derivative of acoustic pressure at a boundary surface, Pa/m
ρ_0	= ambient density, kg/m^3
$\{\Phi\}$	= vector of unknown node pressures, Pa
ω	$= (2\pi f/c_0)$, angular frequency, s^{-1}

Subscripts:

e, s	= exit and source plane
I	= the Ith impedance segment
opt	= Cremer optimum impedance
N, M	= upper indices of summation
q, m	= lower indices of summation

Superscripts:

$*$	= complex conjugate

I. Introduction

The current fleet of large commercial aircraft has successfully achieved FAA noise certifications due, in

*Senior Research Scientist, Computational Modeling and Simulation Branch, Aerodynamics, Aerothermodynamics, and Acoustics Competency. Member of AIAA.

†Research Scientist, Structural Acoustics Branch, Aerodynamics, Aerothermodynamics, and Acoustics Competency.

‡Senior Research Scientist, Structural Acoustics Branch, Aerodynamics, Aerothermodynamics, and Acoustics Competency.

§Senior Research Scientist, Analytical and Computational Structures Branch, Structures and Material Competency. AIAA Fellow.

part, to successful application of passive duct liner treatments to control engine noise. One of the goals of NASA is to develop technologies to improve the sound-absorbing properties of these treatments so that they remain effective in modern, low-drag producing, wide-chord-fan engines.[1] Figure 1 is an illustration of axisymmetric and non-axisymmetric passive duct liner concepts that have potential application to this class of engines. Initially, liner research was centered on the uniform liner that is installed in the engine ducts of the current aircraft fleet. Lansing and Zorumski[2] realized that liners could be made more effective by taking advantage of acoustic impedance changes in axial segments.[3] Consequently, the axially segmented liner was studied extensively by several investigators in the 1970's.[3-8] However, the axially segmented lining configuration was not implemented in modern aircraft engines because their optimum design requires an accurate description of the modal distribution of acoustic energy in the sound source. The problem of determining the modal amplitude and phasing of source modes within wide-chord-fan engine ducts is extremely difficult. In addition, modern inlets may not provide sufficient length-to-diameter ratios (L/D) for efficient use of the axially segmented liner concept.

In the non-axisymmetric liner concepts (see Fig. 1), the duct length is less important because the segmentation is around the circumference instead of along the axis. This is important because the wide-cord-fan engine ducts of today have $L/D < 1$. A beneficial effect of the circumferentially segmented liner configuration was first observed in the mid-1970s by Mani,[9] who simply blocked segments of a uniform liner with strips of aluminum tape. Improved acoustic performance of this configuration was ascribed to mode reconditioning (redistribution of acoustic energy into higher order circumferential modes that are more rapidly suppressed by the liner). Several studies, all based on modal analysis, have followed the experiment of Mani.[10-13] However, the potential of optimized, circumferentially segmented liners has never been fully evaluated because the modal analysis techniques have been based on the attenuation of a single mode.

The potential synergy between axial and circumferential segmentation can be implemented by the checkerboard liner (Fig. 1). To date, no experimental or analytical studies of this liner configuration have been reported. This is at least partially because the checkerboard liner is not amenable to multimodal analysis techniques. The checkerboard liner configuration requires the use of a fully three-dimensional analysis code for accurate modeling. However, three-dimensional aeroacoustic analysis codes are not yet available because of the excessive computational time and memory requirements of the most commonly use equation solvers. It is interesting that although major advances in equation solving methodologies have occurred during the past decade, these advances have yet to be implemented into major aeroacoustic analysis codes.

The work presented in this paper was motivated by the need to implement more efficient equation solvers into aeroacoustic liner design codes and by the need for more effective passive liner treatments for the next generation of aircraft engines. In this paper, computation times and memory requirements for a commonly used solver are compared with those of a state-of-the-art, parallel, sparse solver. The sparse solver is used in conjunction with three optimization algorithms to perform liner optimization studies. The integrity of each algorithm is evaluated by comparing results obtained from each optimization method. We perform an initial assessment of the non-axisymmetric liner concept by comparing its optimum noise attenuation to those of optimized uniform and axially segmented liners. This assessment is performed in a finite-length duct at two source frequencies (4.0 kHz and 7.0 kHz) without flow. All cut-on modes are included in the sound source definition and the analysis uses a geometry corresponding to that of the 'Grazing Incidence Tube' in the NASA Langley Research Center Flow Impedance Test Facility. This geometry was picked to allow convenient experimental collaboration at a later date.

II. Statement of Problem

Figure 2 is a schematic of the three-dimensional duct and right handed coordinate system used to model the grazing incidence impedance tube (GIT). The liner is axially centered in the test section (the section of the duct between the source and exit plane). The upper wall and two sidewalls of the test section are rigid. Strictly speaking, the noncircular geometry of the GIT does not permit a study of circumferentially segmented liners. However, we will allow the liner impedance to be segmented in the spanwise direction (y direction) of the GIT. This will cause scattering of acoustic energy into spanwise modes, thus simulating the effects of circumferential segmentation in a circular geometry. Acoustic waves will be propagated from left to right across the surface of the liner and into a termination section. The test section is 40.64 cm long and has a 5.08 $\times$ 5.08 cm cross section. The source and exit planes are located in rigid-wall sections of the duct, 20.32 cm

from the leading and trailing edge of the liner, respectively. The exit plane acoustic impedance and liner surface acoustic impedance are functions of position. Throughout this paper all impedances are assumed normalized with respect to the characteristic impedance ($\rho_0 c_0$) of the air in the duct. The problem at hand is to determine the liner acoustic impedance that maximizes the noise attenuated by each of the lining concepts.

III. Governing Equations

The mathematical problem is to find the solution to Helmholtz's equation[14]

$$\nabla^2 p + k^2 p = 0 \tag{1}$$

where a time convention $e^{i\omega t}$ is assumed. The boundary condition along the rigid-wall portions of the duct is equivalent to the requirement that the gradient of acoustic pressure normal to the wall vanishes, that is

$$\frac{\partial p}{\partial n} = 0 \tag{2}$$

At the duct exit ($z = L$), the ratio of acoustic pressure to the axial component of acoustic particle velocity must equal the exit acoustic impedance. When expressed in terms of the acoustic pressure, this boundary condition is

$$\frac{\partial p}{\partial z} = \frac{-ikp}{\zeta_e} \tag{3}$$

The liner is assumed to be locally reacting, so that the liner boundary condition is[15]

$$\frac{\partial p}{\partial n} = \frac{ikp}{\zeta} \tag{4}$$

Along the source plane ($z = 0$) of the duct, the sound source pressure, p_s, is known. Therefore, the sound source boundary condition is

$$p = p_s \tag{5}$$

The sound source affects both the optimum liner impedance and the maximum amount of sound attenuated by the lining. For this paper, a modal energy distribution appropriate for a multimodal noise source located in a rigid-wall section of duct

$$p_s = \sum_{q=0}^{N} \sum_{m=0}^{M} A_{qm} \cos(q\pi y/W) \cos(m\pi x/H) \tag{6}$$

is used. We assume that each cut-on source mode has unit amplitude and zero phase ($A_{qm} = 1$). Note that equation (6) is approximately an equal energy modal assumption for which the source in the rigid-wall duct does not vary appreciably with the introduction of the liner. Equations (1)-(6) form a well-posed boundary value problem that can be solved to determine uniquely the acoustic pressure field in the duct. An exact analytical solution for this field is not available for a general input data set; therefore, a numerical method is needed to obtain the solution for this field.

IV. Numerical Solution for Acoustic Pressure

The numerical method used to obtain the solution for the acoustic pressure field is described elsewhere.[16] Only the details necessary for clarity and continuity are presented herein. The solution to equations (1)-(6) is obtained with a conventional Galerkin Finite Element Method using a brick element and linear basis functions. This methodology results in a large, linear, sparse, and symmetric system of complex equations of the form:

$$[A]\{\Phi\} = \{B\} \tag{7}$$

To solve equation (7), a parallel, direct, sparse solver factorizes $[A]$ and then obtains the solution vector using the sequential operations of backward and forward substitution. The solver employs a compressed column storage scheme to reduce storage overhead. Only the nonzero coefficients in the upper triangular part of $[A]$ are stored, along with two pointer arrays which store the column numbers and starting indexes of these nonzero coefficients. To obtain the speed necessary for efficient three-dimensional solutions, the sparse solver uses two accelerators: equation reordering[17,18] to reduce fill during the factorization of $[A]$, and parallelization (the equation solver runs on multiple processors simultaneously).

The sparse solver initially selected to solve equation (7) was a complex version of the Vectored Sparse Solver (VSS).[19] This software package is a commercial version of the NASA-developed general-purpose solver[20] (GPS) that was modified for complex arithmetic and commercialized by the Solversoft Corporation in 1999. However, since that time Silicon Graphics Incorporated (SGI) has developed a parallel sparse solver (ZPSLDLT) that is contained in version 1.4 of the SGI/Cray Scientific Library (SCSL). Studies performed by the authors show that the complex version of VSS and ZPSLDLT have nearly identical time and memory requirements. In addition, ZPSLDLT is readily available to the public whereas VSS is proprietary. Consequently, this paper uses ZPSLDLT to solve equation (7).

V. Objective Function

The segmented liner configurations reported in this paper are restricted to a rectangular geometry with two impedance segments as depicted in figure 3. Each segment of the segmented liner has been purposely designed to have the same cross-sectional area. Additionally, each segmented liner may default to a uniform liner during liner optimization. However, one segmented liner may not default to another (i.e., the checkerboard liner cannot default to the spanwise segmented liner, etc.). The goal is to determine the optimum acoustic impedance of each liner segment that maximizes the noise attenuated by the liner. The authors use the reduction in the sound power from the source to the exit of the duct (F) as an objective function that is maximized to determine the optimal attenuation of the liner. This objective function is a real, positive function, has units of decibels, and is defined as[14]

$$F = 10 \log_{10} \left[\frac{\mathrm{Re}\{\int_0^W \int_0^H E(x,y,0)dxdy\}}{\mathrm{Re}\{\int_0^W \int_0^H E(x,y,L)dxdy\}} \right] \quad (8)$$

$$E(x,y,z) = \frac{ip(x,y,z)}{\rho_0 \omega} \frac{\partial p^*(x,y,z)}{\partial z} \quad (9)$$

Because the acoustic pressure field, p, is known only at a discrete number of points in the duct, the integration in equation (8) is performed numerically using Simpson's rule for numerical integration.

VI. Optimization Methods

We use the attenuation (F) produced by the liner as an objective function and determine the optimum acoustic impedance for each liner segment. For the uniform liner, two parameters are free to vary in the optimization: the acoustic resistance (R_1) and reactance (χ_1). Thus, contours of constant attenuation (referred to here as a contour map (CM)) will be plotted in the impedance plane to determine the global optimum point for the uniform liner. The segmented liners (Fig. 3) have four parameters to vary: the acoustic resistances (R_1, R_2) and the acoustic reactances (χ_1, χ_2). Since it is no longer possible to plot contours of constant attenuation in the four-dimensional space of the segmented liner, we used an iterative two-step procedure to determine the optimum point. The iterative procedure is as follows:

1. Hold the acoustic impedance of the first section ζ_1 equal to that of the optimum uniform liner and use a CM to obtain an optimum ζ_2.

2. Hold ζ_2 at the optimum from step 1 above and use a CM to obtain a new optimum ζ_1.

The above two-step iterative procedure is repeated until the attenuation of the segmented liner converges within some specified tolerance. This optimization method is referred to herein as the iterative contour deformation method (ICDM). A similar procedure to that used here was used by Kraft[8] to design an axially segmented liner. Note that the ICDM is not automated because each iteration must be guided by hand, using results obtained from a CM.

The optimal point for each segmented liner is also obtained using two automated optimization algorithms. The first automated optimization algorithm was a Davidon-Fletcher-Powell (DFP) optimization algorithm.[21] This algorithm has the disadvantages of requiring both an initial starting location and a difference approximation to the gradient of the objective function. Additionally, the method is known to converge to local optima. The second automated optimization algorithm is a genetic algorithm (GA). The GA initializes a random sample of individuals with different parameters to be optimized using evolution via survival of the fittest. In contrast to the DFP, the GA does not require calculation of the gradient of the objective function, nor does it require an initial starting location. Furthermore, when compared with the DFP the GA increases the probability of obtaining a global optimum point. Both optimization methods are constrained so that at the optimum point, each impedance segment contains physically realistic acoustic resistance ($0 \leq R_I \leq 10$) and acoustic reactance ($-10 \leq \chi_I \leq 10$) values. A full description of these two automated optimization algorithms is beyond the scope of this paper. Readers who are unfamiliar with the DFP and GA algorithms are encouraged to consult references 21 and 22.

VII. Results and Discussion

Results in this section are presented with the following three objectives in mind:

1. to demonstrate the efficiency of the sparse solver compared to the most commonly used solver

2. to test the integrity of the optimization methodologies

3. to assess the relative merits of the non-axisymmetric liner concept

The accuracy of the sparse solver has been presented in a previous paper[16] and is not addressed further in this work. All results presented in this

Table 1 Minimum points for resolving cut-on modes

f, kHz	NX	NY	NZ	$NX*NY*NZ$
4.0	6	6	114	4,104
7.0	12	12	200	28,800
11.0	18	18	313	101,412
14.0	24	24	399	229,824
17.0	30	30	484	435,600
21.0	36	36	599	776,304

Table 2 Sparse solver parallel speedup at 14.0 kHz

Number of Processors	Parallel Speedup
2	1.79
4	3.15
8	4.60
16	5.80

paper were computed on an SGI ORIGIN 2000 computer platform using double-precision (64-bit) arithmetic. Note that the physically correct exit acoustic impedance for a multimodal sound source should simulate a nonreflecting termination. Therefore, all liners were designed with an exit acoustic impedance that is nonreflecting to a plane wave source ($\zeta_e = 1$). This exit acoustic impedance was chosen because in an optimally designed liner, higher order modes generated by the sound source will be more rapidly attenuated than the plane wave mode. Therefore, only the plane wave mode is expected to carry significant acoustic energy to the exit plane. Furthermore, this plane wave mode should exit the duct test section with minimal reflections using the chosen exit acoustic impedance.

A. Solver Efficiency Studies

Table 1 shows the minimum number of points required to resolve all cut-on modes (assuming 12 points per wavelength) in the rigid-wall duct for frequencies up to 21.0 kHz. Here, NX, NY, and NZ are the minimum number of equally spaced points in the x, y and z directions, respectively, to resolve all cut-on modes. The current industry practice is to use scale models as small as 1/5 the size of full-scale engines in liner designs. The largest full-scale frequency of interest is typically 4.0 kHz. Thus, the largest frequency of interest for the smallest scale (a 1/5-scale model) is 20.0 kHz. To fully capture this frequency range, the results in table 1 are given up to a frequency of 21.0 kHz. Note that at the highest frequency (21.0 kHz) a matrix order of 776,304 is required to accurately resolve all cut-on modes. Typically, band solvers have been the solver of choice for obtaining the solution to the indefinite, linear system given by equation (7). However, it will be shown that band solvers are too expensive for optimization studies in three spatial dimensions and newer more efficient equation solving methodologies are needed. To better understand the improvement in efficiency of equation solving methods over the past decade, it is helpful to compare the central processor unit (CPU) time and random access memory (RAM) required to obtain the solution to equation (7) using a commonly-used band solver to that of the sparse solver (ZPSLDLT) used in this paper.

The CPU time and RAM for the band and sparse solvers are depicted in figure 4. Results are presented using a dual axis system with the CPU time and RAM referenced to the $Y1$ and $Y2$ axis, respectively. CPU times are given in kiloseconds (ks) and the RAM requirements are given in gigabytes (GB). Results in the figure were computed on a single processor and without equation reordering. As shown in the figure, at higher frequencies, the sparse solver consumes 20% less CPU time (2 hrs less) and only half the RAM of the band solver. Typically, optimizers require thousands of function evaluations (i.e., passes through the solver) to obtain an optimum point. Without further increases in processing speed, it will be impractical to perform optimization studies even with the more efficient sparse solver at the higher frequencies.

The sparse solver has been accelerated with equation reordering to minimize fill during matrix factorization. Figure 5 shows the additional reduction in CPU time that can be obtained using multiple minimum degree (MMD) reordering[17] and nested dissection (ND) reordering[18] on a single processor. The savings in CPU time at the higher frequencies due to equation reordering are clearly evident. Relative to the CPU time without reordering, MMD reordering reduces the CPU time by 14%, whereas a reduction of nearly 64% is achieved with ND reordering. Results in figure 6 show how the reordering schemes reduce the RAM requirements of the sparse solver. Relative to the RAM requirements without reordering, note that at higher frequencies MMD and ND reordering reduces the RAM requirements of the solver by factors of two and three, respectively. Thus, compared with the band solver, the sparse solver with ND reordering reduces the CPU time and RAM requirements by factors of 3.4 and 2.6, respectively, at the higher frequencies.

A second method for reducing the CPU time of the sparse solver is parallelization. Table 2 com-

pares the parallel speedup obtained at a frequency of 14.0 kHz when the solver is run on 2, 4, 8 and 16 processors. The reference timing for computing the parallel speedup is that required for a solution using the parallel version of the sparse solver on a single processor. The solver is observed to run efficiently on up to four processors. Note that the speedup is 1.79 and 3.15 on two and four processors, respectively. There is only a modest improvement in parallel speedup for more than four processors. Furthermore, the sparse solver running on only four processors with ND reordering reduces the CPU time by a factor of nearly eleven when compared with that of the more commonly used band solver (see Fig. 4).

B. Optimization Studies

The uniform, axially segmented, spanwise segmented, and checkerboard liners are designed at two source frequencies (4.0 kHz and 7.0 kHz). At 4.0 kHz the sound source contains three cut-on modes (the (0,0), (1,0), and (0,1) modes), while at 7.0 kHz the sound source contains six cut-on modes (the (0,0), (1,0), (0,1), (1,1), (2,0), and (0,2) modes). Based upon the efficiency studies of the previous section, it was decided to run the sparse solver in parallel on four processors using ND reordering. The initial liner design used a spatial grid that was designed to capture all cut-on modes in a rigid-wall duct for the 7.0 kHz sound source ($NX = NY = 13, NZ = 201$). After the optimum liner was determined, a grid refinement study was conducted, and it was determined that this spatial grid was fine enough to accurately capture the attenuation at the optimum point.

Uniform Liner

Figures 7 and 8 show a contour map of the uniform liner attenuation function at 4.0 and 7.0 kHz, with evenly spaced grids of 100 and 200 points along the resistance and reactance axes, respectively. Note that the attenuation function has a single, well-defined optimum point at each frequency ($\zeta = 1.05 - 0.80i$ and $F = 41.0$ dB at 4.0 kHz; $\zeta = 1.48 - 2.0i$ and $F = 17.2$ dB at 7.0 kHz). The DFP and GA algorithms were also used to obtain the optimum point of the uniform liner. The DFP algorithm was initialized from the following four starting locations in the impedance plane

$$\begin{aligned} \zeta_1 &= 2.5 - 5.0i \\ \zeta_1 &= 2.5 + 5.0i \\ \zeta_1 &= 7.5 - 5.0i \\ \zeta_1 &= 7.5 + 5.0i \end{aligned} \qquad (10)$$

The optimum points obtained with the DFP for each of these starting locations were nearly identical. Generally, the DFP converged to the optimum point in four to eight iterations (depending on the starting location) and each iteration required approximately 4 minutes of CPU time. It should be noted that the GA results were computed using a population size of forty and were observed to converge in forty to fifty generations.

Table 3a Uniform liner results for DFP

f, kHz	R_1	χ_1	F,dB
4.0	0.96	-0.78	45.80
7.0	1.47	-1.91	17.20

Table 3b Uniform liner results for GA

f, kHz	R_1	χ_1	F,dB
4.0	0.97	-0.77	45.60
7.0	1.48	-1.90	17.20

Table 3c Uniform liner results for CM

f, kHz	R_1	χ_1	F,dB
4.0	0.98	-0.80	40.50
7.0	1.45	-1.90	17.10

The uniform liner optimum points achieved with the DFP, GA, and CM are given in tables 3a, 3b, and 3c, respectively. Note that each optimization methodology converged to nearly the same impedance at each frequency, and the optimum attenuations are nearly identical at 7.0 kHz. However, at 4.0 kHz, the DFP and GA optimum attenuations differ from the CM result by approximately 5 dB (nearly 10%). This difference in attenuations for the different algorithms at 4.0 kHz reflects the sensitivity of the attenuation to changes in the second and third decimal digit of the impedance at the optimum point. This indicates that the impedance grid used to construct the CM was not fine enough to determine the optimum attenuation with greater accuracy at the optimum point. It is of interest that maximum attenuation is significantly reduced when the frequency is increased from 4.0 to 7.0 kHz (see tables 3a, 3b, and 3c). The ineffectiveness of the uniform liner at the higher frequencies is a primary reason for investigating the segmented lining concepts. Furthermore, a study of the contour plot tabular data (available from the authors by request) shows that away from the optimum point, the greatest attenuation occurs at resonance ($\chi = 0.0$). However, for finite values of acoustic reactance (and away from the optimum point) the largest attenuation is obtained when the acoustic resistance and reactance

Table 4 Starting locations for the DFP

Location	ζ_1	ζ_2
1	$2.5 - 5.0i$	$2.5 - 5.0i$
2	$2.5 - 5.0i$	$2.5 + 5.0i$
3	$2.5 - 5.0i$	$7.5 - 5.0i$
4	$2.5 - 5.0i$	$7.5 + 5.0i$
5	$2.5 + 5.0i$	$2.5 - 5.0i$
6	$2.5 + 5.0i$	$2.5 + 5.0i$
7	$2.5 + 5.0i$	$7.5 - 5.0i$
8	$2.5 + 5.0i$	$7.5 + 5.0i$
9	$7.5 - 5.0i$	$2.5 - 5.0i$
10	$7.5 - 5.0i$	$2.5 + 5.0i$
11	$7.5 - 5.0i$	$7.5 - 5.0i$
12	$7.5 - 5.0i$	$7.5 + 5.0i$
13	$7.5 + 5.0i$	$2.5 - 5.0i$
14	$7.5 + 5.0i$	$2.5 + 5.0i$
15	$7.5 + 5.0i$	$7.5 - 5.0i$
16	$7.5 + 5.0i$	$7.5 + 5.0i$

have equal magnitude but are opposite in sign.

The optimum acoustic impedance obtained from each of the uniform liner optimization methods (see tables 3a, 3b, and 3c) is nearly identical to the Cremer optimum acoustic impedance[23,24] for the lowest order mode in the infinite duct

$$\zeta_{\text{opt}} = (0.929 - 0.744i)\frac{kH}{\pi} \qquad (11)$$

This result confirms that even for a multimodal source, the optimum acoustic impedance in a finite length duct is still dominated by the least attenuated mode, whose attenuation will be maximized by the Cremer optimum acoustic impedance in an infinite duct. The fact that the current methods reproduce (almost exactly) the Cremer optimum acoustic impedance gives credence to the methodologies used in this paper.

Segmented Liners

The ICDM, DFP, and GA algorithms have been used with the segmented liners in an attempt to obtain optimum attenuations greater than that of an optimum uniform liner. The ICDM was not successful when used with the segmented liners. It was discovered that the ICDM converged to the uniform liner optimum. The failure of the ICDM to converge to an optimum point different than the uniform liner is contrary to the results of reference 8. However, the reader is reminded that the duct geometry, source, and frequency used in this study are significantly different from those used in reference 8. Thus, only the DFP and GA optimization results are presented for the segmented liners. Furthermore, in the segmented

Table 5a Checkerboard liner results for DFP

f, kHz	R_1	χ_1	R_2	χ_2	F, dB
4.0	0.96	-0.77	0.95	-0.78	45.10
7.0	1.47	-1.90	1.46	-1.91	17.20

Table 5b Checkerboard liner results for GA

f, kHz	R_1	χ_1	R_2	χ_2	F, dB
4.0	0.96	-0.78	0.96	-0.77	45.20
7.0	1.48	-1.91	1.47	-1.90	17.20

lining design studies, the DFP was initiated from the sixteen different starting locations given in table 4. In contrast to the uniform liner optimizations, it was found that the segmented liner attenuation function contains multiple local optima. Thus, the DFP results showed great sensitivity to the starting location; therefore, the reported DFP result corresponds to the local optimum with the largest attenuation out of the sixteen starting locations. Tables 5a and 5b compare the optimum attenuation obtained from the DFP and GA algorithm, respectively, for the checkerboard liner. Observe that both the DFP and GA returned the optimum uniform liner design point for the checkerboard liner. Tables 6a and 6b compare the optimum points obtained with the DFP and GA, respectively, for the axially segmented liner. For this liner, both optimization methodologies give nearly the same optimum attenuation, but the optimum impedances predicted (from each method) for the first and second segments are distinctly different. Optimization results for the spanwise segmented liner are given in tables 7a and 7b. Note that for this liner, the two optimization methodologies show significant differences in both the optimum attenuation and the impedance of the second segment at 4.0 kHz. On the other hand, for the 7.0 kHz source, there is only a modest difference in the at-

Table 6a Axially segmented liner results for DFP

f, kHz	R_1	χ_1	R_2	χ_2	F, dB
4.0	0.95	-0.94	0.88	-0.51	48.52
7.0	0.86	-2.29	1.45	-0.70	32.90

Table 6b Axially segmented liner results for GA

f, kHz	R_1	χ_1	R_2	χ_2	F, dB
4.0	0.83	-0.98	1.30	0.03	49.02
7.0	0.91	-2.40	1.30	-0.90	35.60

Table 7a Spanwise segmented liner results for DFP

f, kHz	R_1	χ_1	R_2	χ_2	F, dB
4.0	1.00	-0.80	0.93	-0.76	47.02
7.0	0.69	-2.70	0.83	-0.91	27.72

Table 7b Spanwise segmented liner results for GA

f, kHz	R_1	χ_1	R_2	χ_2	F, dB
4.0	0.91	-0.98	0.76	-0.28	58.80
7.0	0.91	-2.47	1.14	-0.90	31.54

tenuation and impedances at the optimum point.

The most significant result to be gleaned from these segmented liner studies is that the axially segmented and spanwise segmented liners give better attenuation than the uniform liner (see tables 3a, 3b, and 3c). At 4.0 kHz, the optimized axially and spanwise segmented liners give 3.0 dB and 14.0 dB, respectively, of additional attenuation compared with that of the optimized uniform liner. The spanwise segmented liner is clearly a better attenuator of sound than the axially segmented liner when optimized for a 4.0 kHz multimodal source. At 7.0 kHz, the segmented liner designs have nearly the same attenuation but distinct acoustic impedance values. Furthermore, at 7.0 kHz, the segmented liner attenuations are nearly double that of the uniform liner. In general, the DFP optimum design point gives less attenuation than the GA design point for the segmented liners (see tables 6a, 6b, 7a, and 7b).

VIII. Conclusions

Based upon the results of this study, the following conclusions are drawn:

1. The sparse solver (running in parallel on four processors with nested dissection reordering) reduces CPU time and RAM requirements by factors of eleven and five, respectively, when compared with the commonly used band solver.

2. Even for a multimodal noise source in a finite-length duct, the optimum uniform liner acoustic impedance is dominated by the least attenuated mode, in which attenuation is maximized by the Cremer optimum acoustic impedance.

3. The Davidon-Fletcher-Powell (DFP) and genetic algorithms (GA) are useful design tools for the segmented liner, but the iterative contour deformation method (ICDM) returns the uniform liner optimum point.

4. Because segmented liners contain multiple local optima, the genetic algorithm generally leads to a better design than the DFP algorithm.

5. An optimized four-segmented liner with two distinct impedance segments arranged to form a checkerboard pattern is an inferior design compared with an optimum two-segment liner.

6. An optimized spanwise segmented liner is more effective at attenuating sound than an optimized uniform liner. It tends to be more effective at the higher frequencies, and gives attenuations equal to or substantially greater than an optimized axially segmented liner.

The non-axisymmetric liner optimization results are sufficiently encouraging to warrant additional studies. It is important to note that the conclusions of this paper apply only to the source, frequency, and duct geometry for which this study was conducted. Considerable care should be exercised in attempting to generalize these conclusions to other geometries, source structures, and frequencies. Future work is expected to target frequencies in the 8.0 kHz to 21.0 kHz range. Sample calculations presented in this paper (Fig. 5) show that a single function evaluation with the current sparse solver at 21.0 kHz requires nearly an hour of CPU time. Assuming that 1,000 to 2,000 function evaluations are required to obtain the optimum, the current solver would have to be accelerated nearly two orders of magnitude before optimization studies become practical at the highest frequency. Since it is unlikely that the current sparse solver can be accelerated to this degree, it seems reasonable that a response surface methodology[25] will most likely be required for function evaluations at the higher frequencies. Furthermore, if more segments (with distinct acoustic impedance values) are desired at even moderate frequencies, a response surface methodology will most likely be required. In addition, the designs considered in this paper have been concerned with noise suppression at a single frequency. However, the total performance of a lining configuration must be measured by its off-design performance as well. Future investigations should also be concerned with off-design performance.

Acknowledgements

The authors would like to gratefully acknowledge Mr. Jay H. Robinson of the Structural Acoustics Branch at the NASA Langley Research Center for his useful suggestions and assistance with the genetic algorithm.

References

[1] Bielak, G.W., Premo, G.W., and Hersh, A.S., "Advanced Turbofan Duct Liner Concepts," NASA/CR-1999-209002, Feb. 1999.

[2] Lansing, D.L., and Zorumski, W.E., "Effects of Wall Admittance Changes on Duct Transmission and Radiation of Sound," *Journal of Sound & Vibration*, vol. 27, no. 1, March 1973, pp. 85-100.

[3] Zorumski, W. E., "Acoustic Theory of Axisymmetric Multisectioned Ducts." NASA TR R-419, June 1974.

[4] Motsinger, R.D., Kraft, R.E., Paas, J.E., and Gahn, B.M., "Analytical and Experimental Results of Some Segmented Liner Acoustic Performance Studies for High Mach Number Inlets." NASA CR-2882, June 1974.

[5] Quinn, D.W.,"Attenuation of the Sound Associated with a Plane Wave in a Multisectioned Duct." AIAA Paper No. 75-496, March 1975.

[6] Sawdy, D.T., Beckmeyer, R.J., and Pattern, J.D., "Optimum Segmented Acoustic Liners for Flow Ducts." Paper D6, 90th Meeting Acoustical Society of America (San Francisco, CA, Nov. 1975).

[7] Lester, H.C., and Posey, J.W., "Optimum One-Section and Two-Section Circular Sound Absorbing Duct Liners for Plane-Wave and Monopole Sources Without Flow," NASA TN D-8348, 1976.

[8] Kraft, R.E., "Theory and Measurement of Acoustic Wave Propagation in Multi-Segmented Rectangular Flow Ducts," A PhD Thesis, University of Cincinnati, 1976.

[9] Mani, R., "Acoustic Duct with Peripherally Segmented Acoustic Treatment," U.S. Patent 3,937,590, Feb. 1976.

[10] Astley, R.J., Walkington N.J., and Eversman, W., "Transmission in Flow Ducts with Peripherally Varying Linings," AIAA Paper 80-1015, June 1980.

[11] Watson, W.R., "Circumferentially Segmented Duct Liners Optimized for Axisymmetric and Standing-Wave Sources," NASA TP-2075, Sept. 1982.

[12] Watson, W.R., "An Acoustic Evaluation of Circumferentially Segmented Duct Liners," *AIAA Journal*, vol. 22, no. 9, Sept. 1984, pp. 1229-1233.

[13] Parrott, T.L., and Watson, W.R.,"Comparison of Measured and Calculated Mode Redistribution Associated with Spinning Mode Transmission Through Circumferentially Segmented Lined Ducts," NASA TM-84576, March 1983.

[14] Morse, P. M., and Ingard, K. U., *Theoretical Acoustics*, McGraw-Hill, New York, 1968, pp. 495–496.

[15] Myers, M. K., "On the Acoustic Boundary Condition in the Presence Of Flow," *Journal Of Sound & Vibration*, vol. 71, no. 3, 1980, pp. 429–434.

[16] Watson, W.R., "Three-Dimensional Rectangular Duct Code with Application to Impedance Eduction," *AIAA Journal*, vol. 40, no. 2, Feb. 2002, pp. 217–226.

[17] Liu, J., "Modification of the Minimum-Degree Algorithm by Multiple Elimination," *Association for Computing Machinery, Transaction on Mathematical Software*, Vol. 11, 1985, pp. 141–53.

[18] George, A., and Liu, J., *Computer Solution of Large Sparse Positive Definite Systems*, Prentice-Hall, Inc., Englewood Cliffs, NJ, 1981, chap. 5 & chap. 10.

[19] VSS Sparse Linear Equation Solver, http://Solversoft.Com.

[20] Storaasli, O.O., "Performance of NASA Equation Solvers On Computational Mechanics Applications," *Proceedings of the 37th AIAA/ASME/ASCE/ANS/ASC Structures, Structural Dynamics and Materials Conference*, 1996, pp. 1680–85.

[21] Stewart, G.W. III, "A Modification of Davidon's Minimization Method to Accept Difference Approximations of Derivatives," *Journal of ACM*, vol. 14, no. 1, Jan. 1967, pp. 72–83.

[22] Goldberg, D., *Genetic Algorithms in Search, Optimization and Machine Learning*, Addison-Wesley, New York, NY, 1989, pp. 75–147.

[23] Cremer, L., "Theory of Sound Attenuation in a Rectangular Duct with an Absorbing Wall and the Resultant Maximum Attenuation Coefficient," McDonnell-Douglas Corp., Report No. MCD-J6630, July, 1974. Translated from *Acoustics*, vol. 3, no. 2, 1953, pp. 249-263.

[24] Tester, B.J., "The Optimization of Modal Sound Attenuation in Ducts, in the Absence of Mean Flow," *Journal of Sound & Vibration*, vol. 27, no. 4, 1973, pp. 477-513.

[25] Montgomery, D.C. *Design and Analysis of Experiments*, 3rd ed., John Wiley & Sons, New York, NY, 1991, chap. 16.

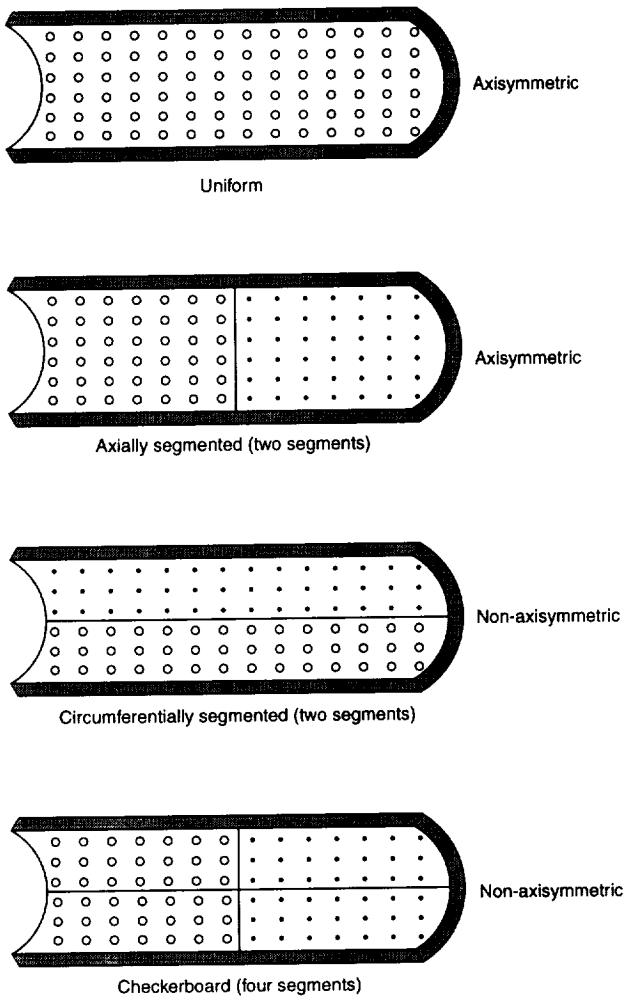

Fig. 1 . Passive liner impedance concepts.

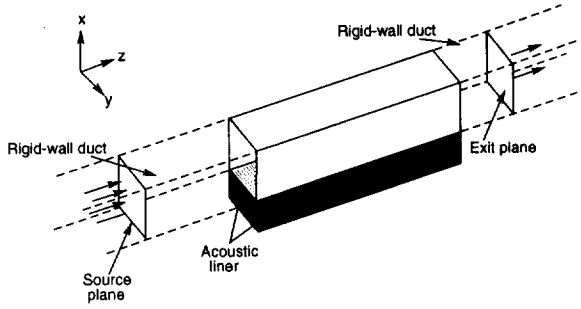

Fig. 2. Three-dimensional duct and coordinate system.

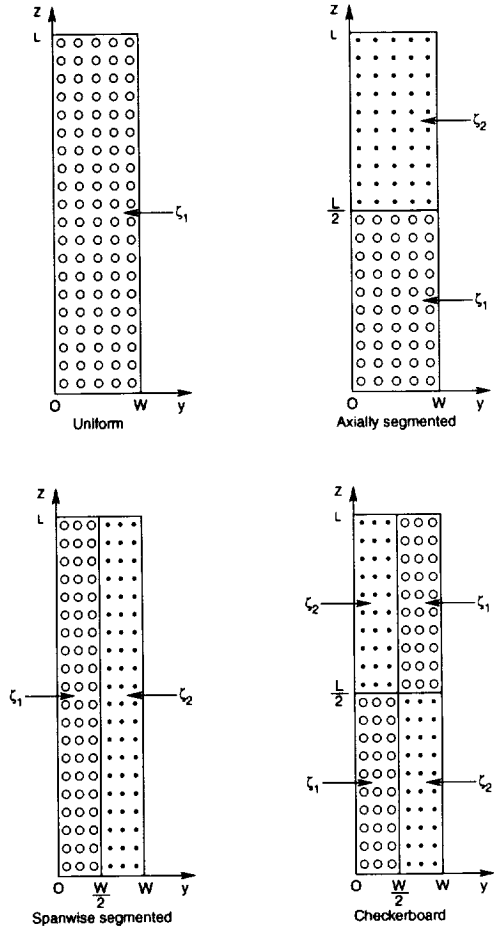

Fig. 3. Schematic of rectangular duct liner configurations.

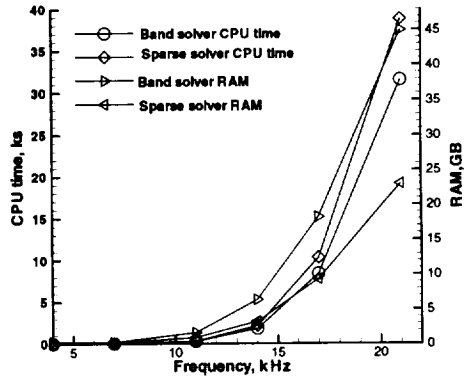

Fig. 4. Single processor CPU times and RAM requirements for the band and sparse solvers.

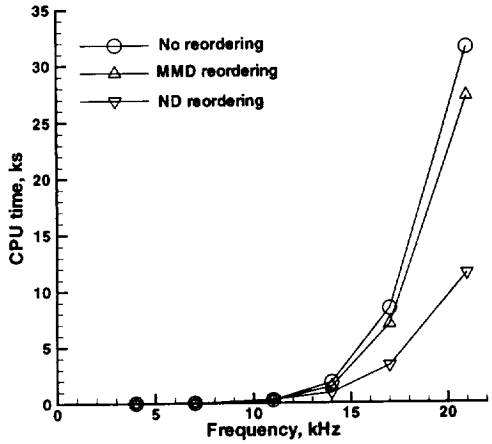

Fig. 5. Effects of equation reordering on CPU times of the sparse solver.

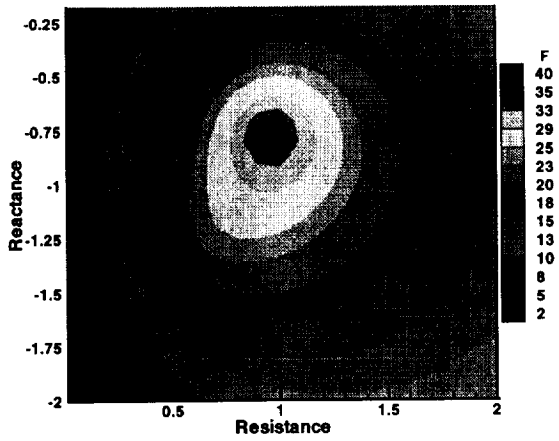

Fig. 7. Uniform liner contour map for the 4.0 kHz source.

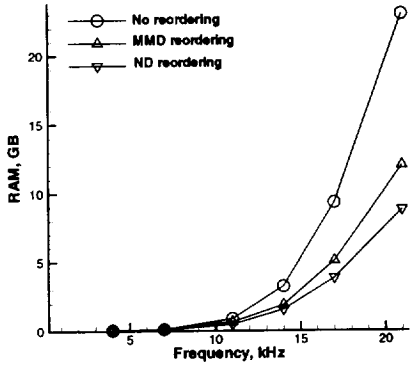

Fig. 6. Effects of equation reordering on RAM requirements of the sparse solver.

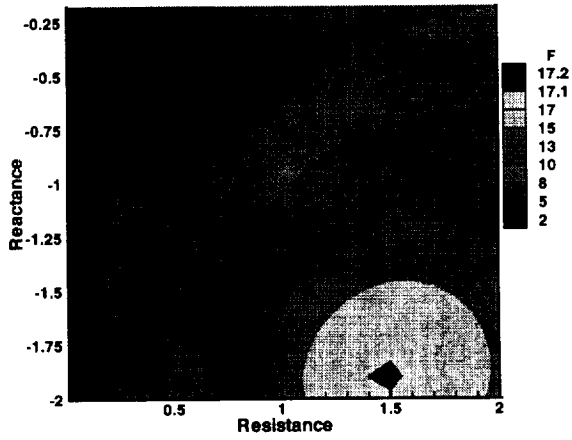

Fig. 8. Uniform liner contour map for the 7.0 kHz source.